Journal of Catalysis 284 (2011) 126–137

Contents lists available at ScienceDirect

Journal of Catalysis

journal homepage: www.elsevier.com/locate/jcat

Probing elementary steps of nickel-mediated bond activation in gas-phase reactions: Ligand- and cluster-size effects ☆

Maria Schlangen *, Helmut Schwarz *

Institut für Chemie, Technische Universität Berlin, Straße des 17. Juni 115, 10623 Berlin, Germany

ARTICLE INFO

Article history:
Available online 13 May 2011

This Review Article is dedicated, with admiration, to Professor Günther Wilke, one of the founding fathers of contemporary organo-nickel chemistry (see, e.g.: G. Wilke, Pure Appl. Chem. 17 (1968) 179).

Keywords:
Bond activation
Catalysis
Cluster-size effects
Gas-phase chemistry
Ligand effects
Nickel
Reaction mechanism
Transition metals

ABSTRACT

Mass-spectrometry-based experiments, complemented by computational studies, are presented which demonstrate the richness of nickel-containing reagents when employed in various bond-activation processes and conducted under single-collision conditions. We will address the chemistry of "naked" atomic Ni^+, the dramatic effects of ligands L or of the size of clusters, which they exhibit in thermal reactions of NiL^+ or Ni_n^+ (n = 2–30). Special emphasis will be paid to identify elementary steps and to uncover mechanistic principles; as an example, various aspects of the face-selective dehydrogenation of cyclohexane by homo- and heteronuclear cluster-ion dimers are discussed in some detail for the first time.

1. Introduction

Exploitation of the distinct chemical features of transition metals, owing to their unique electronic configuration, constitutes the basis of heterogeneous catalysis [1]. Although the *d*-block elements offer an impressive variety of catalytic properties, this versatility is confronted with an enormous number of challenges, which in many cases prevent the realization of a catalytic sequence. Variation of surface textures and the combination of different transition metals are, among others, possible means to enhance the performance and to enlarge the number of given catalytic systems. For example, synergistic effects of different transition metals proved crucial to bring about efficient C–N coupling reactions of methane and ammonia in gas-phase experiments with bimetallic heteronuclear cluster cations not being achieved by their homonuclear analogs [2–4]. Further, it is well-known that surface defects, which often serve as the active site for chemical reactions, have in common with support-free transition-metal clusters an electronic unsaturation; therefore, these clusters may act as suitable models to study the intrinsic properties of catalysts.

As demonstrated repeatedly, gas-phase studies provide a powerful experimental arsenal to uncover both elementary steps and mechanistic details of reactions under well-defined conditions without being obscured by difficult-to-control or poorly understood solvation, aggregation, counterions, and other effects [5–13]. These studies on "isolated" reactants render an ideal arena for probing experimentally the energetics and kinetics of a chemical reaction in an unperturbed environment at a molecular level and to characterize in detail intermediates that have previously not been within the reach of conventional condensed-phase techniques. Of course, as a result of the net Coulomb charge of the ions studied in mass-spectrometry-based experiments as well as the absence of counterions and solvation, these "naked" species will, on principal ground, never account for the precise mechanisms which prevail in the condensed phase; therefore, a direct transfer of the insight arrived at is, in general, not warranted. Nevertheless, studies of this kind have proved meaningful, for they provide a *conceptual* framework to analyze the reactions in question. In fact, the DEGUSSA process, i.e. the platinum-mediated coupling of CH_4 and NH_3, to generate HCN [14], may serve as a good example. Mass-spectrometry-based experiments [2–4] suggested the key

☆ Part of the material described here has been presented by the authors at the IDECAT Conferences on Catalysis, Porquerolles, 2009 (HS) and 2010 (MS).

* Corresponding authors. Fax: +49 (0) 314 21102.
E-mail addresses: Maria.Schlangen@mail.chem.tu-berlin.de (M. Schlangen), Helmut.Schwarz@mail.chem.tu-berlin.de (H. Schwarz).

0021-9517/$ - see front matter © 2011 Elsevier Inc. All rights reserved.
doi:10.1016/j.jcat.2011.03.020

role of CH_2NH as a crucial transient, and the existence of this species was later verified by means of *in situ*-photoionization studies [15].

In this Review Article, we will focus on various aspects related to the gas-phase chemistry of nickel. We will refrain from describing the experimental and computational methodologies, as these are available from the extensive references given; rather, emphasis will be paid to the elucidation of the (often) intriguing mechanisms. In brief, most of the experiments, complemented by either DFT- or wave-function-based electron-structure calculations, employ advanced, if not state-of-the-art, mass-spectrometric methods that allow the generation of mass-selected, electronic ground-state species, and to explore their chemistry under properly defined (mostly) single-collision conditions.

On various grounds, the element Nickel has been chosen as a representative transition metal. Historically, its catalytic activity was already described as early as 1902 by Sabatier and Senderens [16] in the context of methanation of CO; later, in the initial Fischer–Tropsch synthesis nickel was also employed [17,18]. Further, nickel salts proved to play a crucial role (''Nickel-Effekt'') in the early days of Ziegler's pioneering, ground-breaking work on olefin polymerization [19–21], and the element also exhibits an extraordinary versatility in cyclooligomerization, cycloaddition as well as coupling reactions [22–25]. The growing, renewed interest in nickel-mediated enzymatic transformations and in chemical biology has become obvious in the last decades [26]. It is the intention of this Review to highlight the very special position which both ''naked'' [27] and ligated nickel ions[1] also occupy in an impressive variety of gas-phase reactions [28] some of which have a bearing on catalysis.

The organization of the article will be such that in the first part the focus will be on mononuclear nickel-containing species. Here, we will describe briefly the chemistry of ''bare'' Ni^+ and then, in some more detail, the often dramatic effects of ligands L in NiL^+ complexes in their reactions with structurally simple substrates. For a few systems, examples of genuine gas-phase catalysis brought about by *individual* Ni^+ atoms will be presented, e.g., the direct conversion $CH_4 \rightarrow CH_3OH$. In a second chapter, we shall deal with the role of cluster-size effects as well as that of the chemical composition of small homo- and heteronuclear clusters on bond-activation processes. As a specific example, we shall discuss unpublished experimental findings together with mechanistic aspects related to the metal-mediated, face-selective dehydrogenation of cyclohexane. Finally, brief mentioning will be made in the context of *remote functionalization* [29,30] brought about by diatomic homo- and heteronuclear metal-cluster ions when compared to ''naked'' transition-metal ions.

2. Mononuclear Ni-containing systems

2.1. Reactions of ''naked'' atomic Ni^+

Under thermal conditions, ground-state atomic Ni^+ ($3d^9$, $^2D_{5/2}$) is rather reluctant to react with small, inert molecules, e.g., molecular hydrogen [31]. Also, in the ion/molecule reaction with water only inefficient clustering takes place [32]; bond activation resulting in, e.g., the formation of NiO^+ and H_2 (or of NiS^+ and H_2 from the Ni^+/H_2S couple) are calculated to be rather endothermic [33,34] and thus not accessible at ambient conditions. The same holds true for the Ni^+/NH_3 couple; here, endothermic formation of $Ni(NH_2)^+$ and NiH^+ occurs only at elevated kinetic energy and $HNi(NH_2)^+$ serves as a common intermediate [35]. Similarly, room temperature activation of CH_4 cannot be brought about by ''cold'' atomic Ni^+; rather, one observes clustering [36,37]. However, upon kinetic excitation the formation of NiH^+, $Ni(CH_2)^+$, and $Ni(CH_3)^+$ takes place [38]. For the reaction of Ni^+ and SiH_4, Eq. (1), in an endothermic reaction proceeding through a common Ni^{III} insertion intermediate, an energy-dependent branching occurs. At low internal energy, dehydrogenation prevails while at higher energy the heterolytic cleavage of the Ni–Si bond gains importance [39].

$$Ni^+ + SiH_4 \longrightarrow [H{-}Ni{-}SiH_3]^+ \longrightarrow \begin{cases} Ni(SiH_2)^+ + H_2 \\ NiH + SiH_3^+ \end{cases} \quad (1)$$

The scenario changes for larger hydrocarbon substrates; in addition to a generally increased reactivity one encounters a mechanistically rather interesting situation in the $Ni^+/n\text{-}C_4H_{10}$ and $Ni^+/n\text{-}C_6H_{14}$ systems. While bare, atomic metal ions often bring about 1.2-dehydrogenation of larger alkanes, the reaction of Ni^+ with *n*-butane proceeds via selective 1.4-dehydrogenation (as evidenced by the loss of D_2 from $CD_3CH_2CH_2CD_3$) to afford a bisethylene complex $Ni(C_2H_2D_2)_2^+$ [40]. The reaction commences with an oxidative insertion of the metal into the central C–C bond of the substrate [40] to be followed by two sequential β-hydrogen-atom transfers via multi-centered transition states [41,42] and, finally, completed by the liberation of molecular hydrogen. Based on rather extensive labeling experiments, two competing modes of 1.4-hydrogen elimination control the dehydrogenation of $n\text{-}C_6H_{14}$ by Ni^+ involving specifically and pairwise the positions C(1)/C(4) and C(2)/C(5), respectively [43].

Insight into the energetic dependence and the ordering of sequential C–H vs. C–C bond activation has been provided by experimental and computational studies for the Ni^+-mediated demethanation of acetaldehyde, Scheme 1 [44–46].

These studies reveal that the jet-cooled encounter complex **1** upon photon absorption decomposes via competitive, consecutive reactions. At higher internal energies (>200 kJ mol^{-1}) both paths are accessible, and the rate-limiting step corresponds to k_4, i.e., the coupled methyl migration and the reductive elimination of CH_4. Below this energy threshold, only the sequence C–C bond activation/hydrogen-atom migration (**1** → **2** → **4**) plays a role with the step **2** → **4** being rate-limiting. Related computational/experimental studies have also been conducted for the $Ni^+/(CH_3)_2CO$ system [47,48]. Remarkably, both the Ni^+-mediated demethanation of CH_3CHO, Scheme 1, as well as the generation of C_2H_6 from $Ni^+/(CH_3)_2CO$, Eq. (2), require significantly less energy than the metal-free, thermal decomposition of these two substrates; thus, the presence of ''bare'' Ni^+ opens up energetically favorable pathways, which is precisely what a catalyst is supposed to do.

$$[Ni\cdots OC(CH_3)_2]^+ \rightarrow [CH_3C(O)-Ni-CH_3]^+ \rightarrow Ni(CO)^+ + C_2H_6 \quad (2)$$

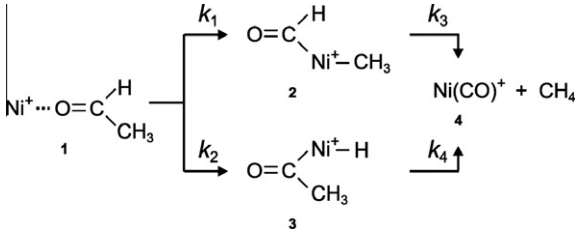

Scheme 1. Reaction network for the Ni^+-mediated demethanation of acetaldehyde.

[1] For an excellent, exhaustive review covering the literature from 1996 to 2006 with a focus on the thermochemistry and bonding features of Ni^+ and Ni_2^+ containing ions in the gas phase, see: O. Mo, M. Yañez, J.-Y. Salpin, J. Tortajada, Mass Spectrom. Rev. 26 (2007) 474.

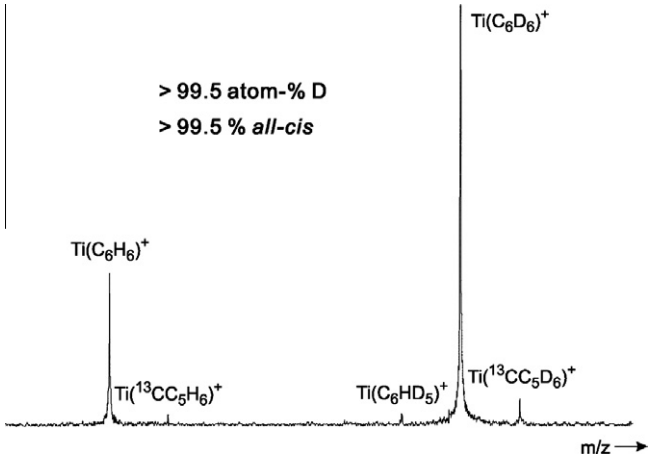

Fig. 1. Partial FT-ICR mass spectrum of the triple-dehydrogenation region for the reaction of bare Ti^+ with [*all-cis*-1,2,3,4,5,6,-D_6]-cyclohexane (adapted from Ref. [50]).

Initial C–C bond activation rather than oxidative insertion of the metal in a C–H bond is also a hallmark in the selective gas-phase chemistry of atomic Ni^+ with *n*-pentylbenzene. Based on extensive labeling studies, specific cleavage of the benzylic C–C bond is followed by loss of C_4H_8 from the side chain [49].

A truly remarkable face selectivity in the dehydrogenation of cyclohexane has been observed in the reactions of this substrate with "bare" first-row transition-metal cations [50]. As shown in Fig. 1, atomic Ti^+ converts C_6H_{12} quantitatively to C_6H_6 (benzene), and the study of [*all-cis*-1,2,3,4,5,6-D_6]-cyclohexane reveals liberation of $3H_2$ and $3D_2$, but no HD. Thus, the components of molecular hydrogen (deuterium) originate from the same face of the ring. For most of the transition metals M^+ (Sc^+–Ni^+) studied, the first dehydrogenation occurs stereospecifically in terms of a 1.2-*syn*-elimination. Further, the extent of consecutive dehydrogenations, i.e., $C_6H_{12} \rightarrow C_6H_{10} \rightarrow C_6H_8 \rightarrow C_6H_6$, is controlled by the nature of the transition metal. For example, Sc^+ and Ti^+ bring about triple loss of molecular hydrogen, while Ni^+ favors the conversion $C_6H_{12} \rightarrow C_6H_{10}$ with smaller contributions of double dehydrogenation and minor products due to C–C bond cleavage. The overall kinetic isotope effects (KIEs) for the single and triple dehydrogenation, i.e., k_{H_2}/k_{D_2} and k_{H_6}/k_{D_6}, respectively, center around 4.0.

The systems Ni^+/CXS (X = O, S) serve as examples for the cleavage of a double-bond. Once more, insertion of the metal rather than a direct, one-step "harpoon" mechanism occurs in the initial phase of the reaction giving rise to an $[S–Ni–C=X]^+$ intermediate from which, in an endothermic step, CX is liberated [51].

2.2. Ligand effects in nickel-mediated reactions

While the addition of *closed*-shell ligands L, e.g., H_2O, CO, or N_2 in general lowers the reactivity of NiL^+ in comparison with atomic Ni^+ [28], ligation with *open*-shell ligands to form formal Ni^{II} species is often accompanied with a drastic increase in reactivity. Among the many examples studied, we first select three representative classes of covalent $M(L)^+$ species (L = H, CH_3, F) for a brief discussion focusing on mechanistic aspects in their thermal gas-phase reactions with methane. In addition, we shall present some remarkable findings which point to the role that electronic structure modifications play.

2.2.1. The NiH^+/CH_4 system

While Ni^+ does not activate CH_4 at ambient conditions, in the NiH^+/CH_4 couple rather efficient ligand exchange, Eq. (3), occurs at a temperature as low as 80 K [52]. Labeling experiments reveal that 93% of the encounter complex undergo a direct ligand switch and only 7% are subject to hydrogen scrambling between the Ni-bonded hydride and the H-atoms of the incoming ligand [53,54]. A KIE = 1.7 has been derived for the direct ligand switch; thus, cleavage of a C–H (D) and making the H–H (D) bond contribute to the rate-limiting step.

$$NiH^+ + CH_4 \rightarrow Ni(CH_3)^+ + H_2 \quad (3)$$

As to the mechanism, B3LYP-based calculations, Fig. 2, demonstrate that this reaction constitutes a textbook example for the operation of a two-state reactivity (TSR) scenario [55–59] in a strictly *thermal* reaction. Here, crossings mediated by spin-orbit coupling between the high-spin $^3\Delta$ ground-state and the low-spin excited $^1\Sigma^+$ state of NiH^+ occur at both the entrance and exit channels of the reaction. This change of spin states enables the system to by-pass the energetically inaccessible **TS 5/6** on the ground-state surface. Further, theoretical work suggests that the reaction proceeds via σ complex-assisted metathesis (σ-CAM) [60] as shown in Fig. 2; the alternative mode of a sequence of oxidative addition/reductive elimination (OA/RE) is not accessible energetically [54].

2.2.2. The $Ni(CH_3)^+/CH_4$ system

The degenerate, rather inefficient (ca. 7% of the collision rate) ligand exchange has been studied in quite some detail [61]. While in the couple $Ni(CH_3)^+/CD_4$ the contribution of the direct ligand switch $CH_3 \rightarrow CD_3$ is rather high, nevertheless, single and double H/D atom exchange between the incoming and outgoing groups precedes the actual ligand switch. According to DFT calculations, once more a σ-CAM mechanism in combination with a TSR scenario are operative. As the energetically lowest pathway is still by 28 kJ mol^{-1} higher in energy than the entrance channel, a small reaction efficiency results.

2.2.3. The NiF^+/CH_4 system

In contrast to the unreactive Ni^{II} halides NiL^+ (L = Cl, Br, I), diatomic NiF^+ brings about exothermic ligand exchange $F \rightarrow CH_3$ [62]; further, the existence of an intramolecular KIE of 3.3 has been derived from the reaction of NiF^+ with CH_2D_2 [28]. The view that breaking the C–H(D) and making the F–H(D) bonds contribute to the rate-limiting step is also supported by DFT calculations, Fig. 3, which favor a spin-conserving σ-CAM reaction on the high-spin triplet-ground state (**7** → **8**). Interestingly, a TSR scenario does not need to be invoked for this particular system – in distinct contrast to the NiH^+/CH_4 couple, Fig. 2 vs. Fig. 3. What is the origin of this deviating behavior? Generally speaking, σ-CAM reactions favor low-spin states [60,61] because of the better ability to accept electrons delivered by the incoming σ-C–H bond of CH_4. In a triplet state, this electron flow experiences a somehow repulsive interaction. Consequently, for a system with a relatively small triplet-singlet energy gap of the reactants, as for NiH^+, a TSR scenario involving the (excited) singlet state gets favored. For NiF^+, however, this energy gap is much too large (>200 kJ mol^{-1}) to play a role; however, as the strongly electron-withdrawing F ligand reduces the electron density at the Ni center, the repulsive interaction decreases. Consequently, the ligand exchange can proceed on the high-spin triplet-ground state. This way of reasoning is supported by an analysis of the *Mulliken* charges at the Ni center in NiL^+, amounting to 0.69 for NiH^+ and 0.91 for NiF^+.

2.2.4. The NiL^+/RH systems (L = F, Cl, Br, I; R = CH_3, C_2H_5, *n*-C_3H_7, *n*-C_4H_9)

Based on a rather extensive reactivity screening [62], general trends have been uncovered for the rich gas-phase chemistry of the above-mentioned NiL^+/RH couples. The reactions observed

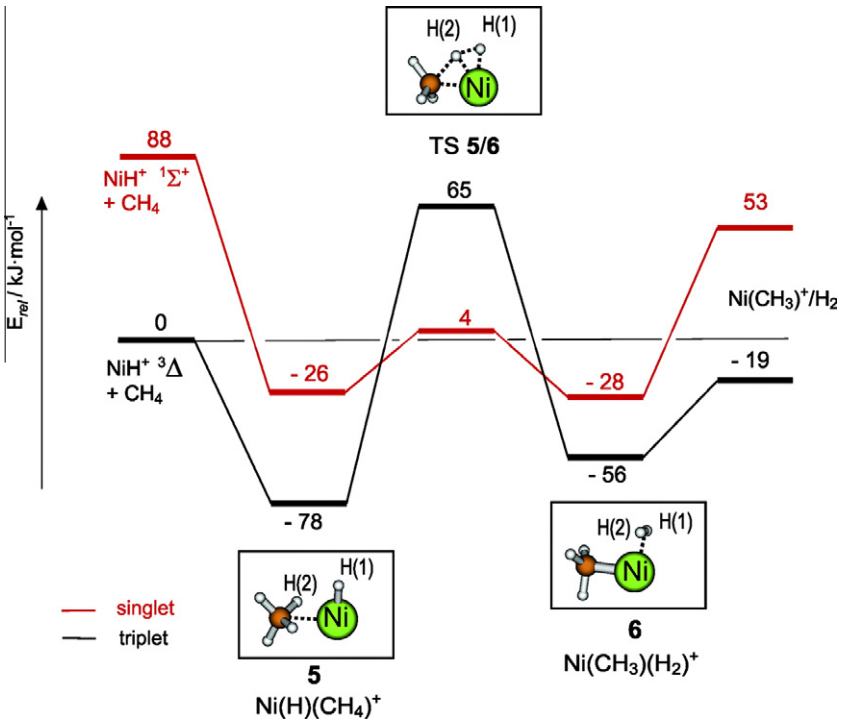

Fig. 2. B3LYP-based, zero-point energy corrected energy diagram for the reaction of NiH^+ and CH_4 employing a TZVP basis set (adapted from Ref. [54]).

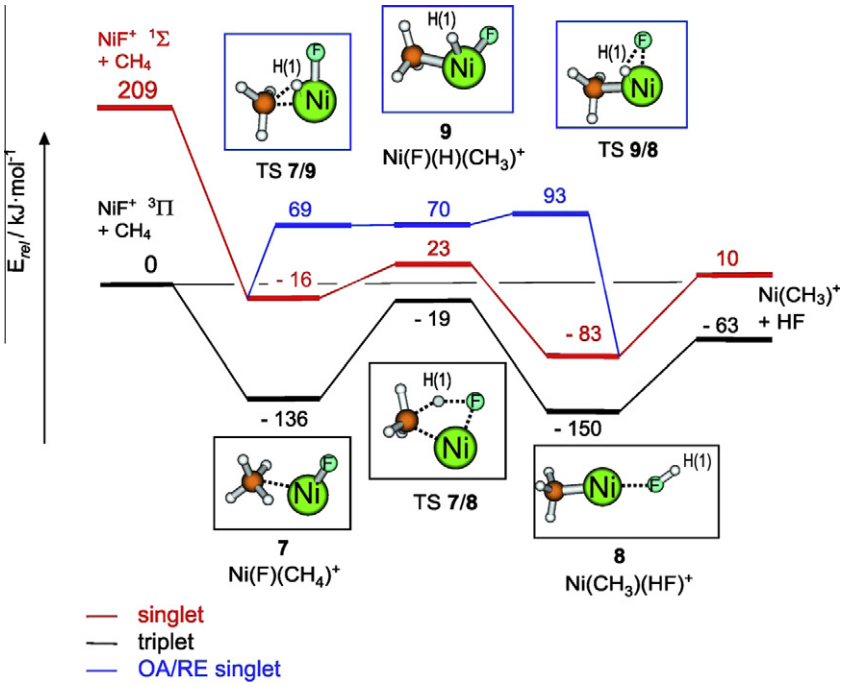

Fig. 3. B3LYP-based, zero-point energy corrected energy diagram for the reaction of NiF^+ and CH_4 employing a TZVP basis set (adapted from Ref. [54]).

can be classified in three categories: (a) bond activation of the organic substrate RH without obvious occurrence of Ni–L bond cleavage, that is, the losses of H_2, CH_4, and C_2H_6 which formally lead to the corresponding NiL^+/olefin complexes; (b) processes involving Ni–L bond scission, namely the evaporation of HL, HL/H_2, and HL/CH_4, affording nickel-allyl or nickel-alkenyl cations, respectively, and (c) eliminations of neutral RNiL units (R = H, CH_3), concomitant with the generation of the corresponding carbenium ions. Fig. 4 shows the relative reaction efficiencies of channels (a–c) for all systems investigated.

The following generalizations have been derived: (1) The reactivity of NiL^+ follows the order L = F > Cl ≅ Br > I and increases with the size of the substrate RH. (2) In the elimination of HL, this reaction channel decreases in going from NiF^+ to NiI^+. A reversed trend is observed in the losses of small closed-shell neutral molecules, that is, H_2, CH_4, and C_2H_6; this channel dominates the gas-phase

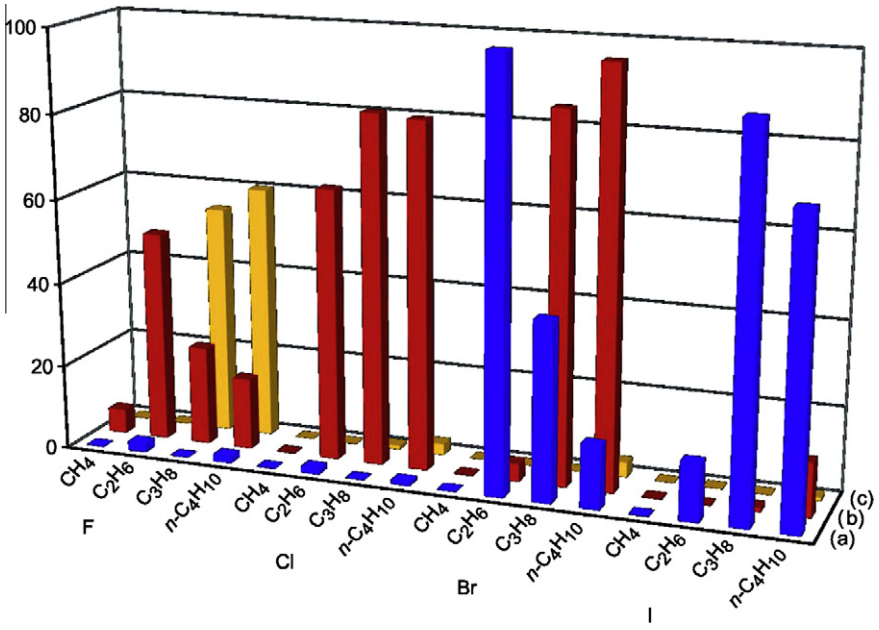

Fig. 4. Relative reaction efficiencies for (a) activations of the alkane without apparent cleavage of the Ni–L bond (■), (b) reactions concomitant with Ni–L bond cleavage (■), and (c) losses of neutral RNiL species (■). Here, the data are weighted with the relative rates and renormalized to a maximal reaction efficiency of 100 for the dehydrogenation of ethane by $NiBr^+$ (adapted from Ref. [62]).

chemistry of NiI^+/RH. (3) The formal inner-sphere electron transfer, i.e., the delivery of hydride or methanide ions from the hydrocarbons to NiL to generate *neutral* HNiLi (or CH_3NiL) and a carbenium ion is reserved for NiF^+, and constitutes the major pathway in the reactions of NiF^+ with C_3H_8 and *n*-C_4H_{10}. It is not observed for any of the NiI^+/RH couples studied. (4) Further, quite impressive, if not unprecedented regioselectivity patterns were uncovered for some of the systems. For example, for NiF^+/C_3H_8, the selectivity of the hydride transfer is as large as 360 (!) in favor of the secondary C–H positions.

2.2.5. "Roll-over"-cyclometalation

Remarkable metal- and ligand-dependent effects were encountered in the context of "roll-over"-cyclometalation reactions [63–65]. While the platinum complex of **10-M** (M = Pt) upon collisional activation undergoes loss of CH_4 to specifically generate the "roll-over" product **11**, due to weaker M–C bonds and higher barriers for the H-transfer from C(3) in a "roll-over" cyclization, the corresponding nickel and palladium complexes **10-M** (M = Ni, Pd) decompose via simple M–C bond cleavage to produce **12**, Scheme 2. The nature of the covalently bonded ligand (L = F, Cl, Br, I, O, Ac rather than CH_3) in **10** matters as well, and an extreme case is given by the nickel fluoro-complex **13** for which the loss of HF is observed exclusively. "Roll-over" cyclometalation amounts to <10% while >90% of the hydrogen in HF originates from C(6), i.e. **13** → **14**. The analogous complex $[Ni(Cl)(bipy)]^+$ undergoes competitive losses of Cl and HCl upon collisional activation, and for the bromo- and iodo complexes only homolytic cleavage of the Ni–halogen bond takes place. In the elimination of HCl from $[Ni(Cl)(bipy)]^+$, >60% of the hydrogen atoms originate from C(3),

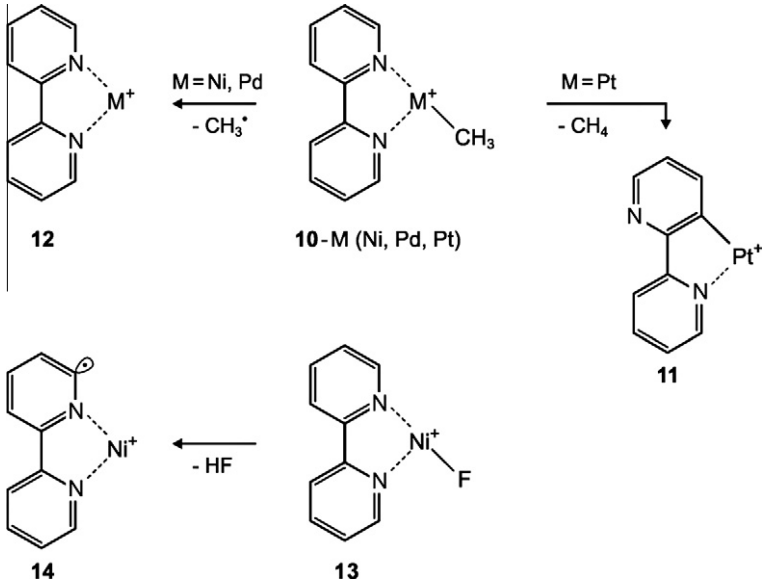

Scheme 2. "Roll-over" cyclometalation vs. other decomposition routes of M^{II}-2,2′-bipyridine complexes (M = Ni, Pd, Pt).

and the remaining from C(4, 5, 6), as inferred from labeling experiments [64]. Extensive DFT calculations have been conducted to unravel, with some success, the underlying grounds of this distinct metal- and ligand-dependent bond activation scenarios [64,65].

2.2.6. The $Ni(H)(OH)^+$ chemistry

This seemingly simple nickel complex and its gas-phase chemistry have generated quite some interest in the context of C–H and O–O bond activation. The "formal" Ni^{III} cation (see below) can be generated by electrospray ionization (ESI) of a NiI_2 solution in a mixture of CH_3OH/H_2O [66]. As to its genesis, the hydridic H-atom of $Ni(H)(OH)^+$ stems from the methyl group of CH_3OH, whereas the hydroxyl group is provided by water. As shown in Fig. 5, complex $Ni(H)(OH)^+$ can be easily distinguished from isomeric $Ni(H_2O)^+$; the latter, a genuine Ni^I-water complex, upon collisional activation gives rise to H_2O loss, Fig. 5a, while isomeric $Ni(H)(OH)^+$ undergoes preferential cleavage of the Ni–(OH) bond, Fig. 5b. The structural assignment is further supported by structure-specific ion/molecule reactions of the two isomers with D_2O and D_2 [66]. Most interestingly, in the thermal reaction of the two isomers with CH_4 it is only $Ni(H)(OH)^+$ which brings about ligand-exchange H → CH_3, Fig. 6b; the Ni^I–water complex is, as expected, completely inert, Fig. 6a.

$Ni(H)(OH)^+$ also exhibits a unique reactivity in its thermal gas-phase reaction with molecular oxygen [67,68], transformations which are of broader interest with regard to a molecular-based understanding of oxygen activation by metal hydride complexes [69]. While the actual structures of the ionic products generated from the $Ni(H)(OH)^+/O_2$ couple remain by and large unknown, details about the origin of the neutral molecules liberated in the course of the reaction can be extracted from labeling experiments, which reveal an extraordinarily high selectivity, Fig. 7. For example, in the formation of HO_2 the OH group of $Ni(H)(OH)^+$ is not involved at all. Similarly, the OH radical liberated contains the hydridic Ni-bonded H atom and an oxygen atom from O_2; finally, the O-atom eliminated from the encounter complex also stems from O_2. Thus, O–O bond activation is crucial, and the network depicted in Scheme 3 summarizes a mechanistic scenario which is consistent with the experimental findings and which has been confirmed by extensive UB3LYP calculations [68].

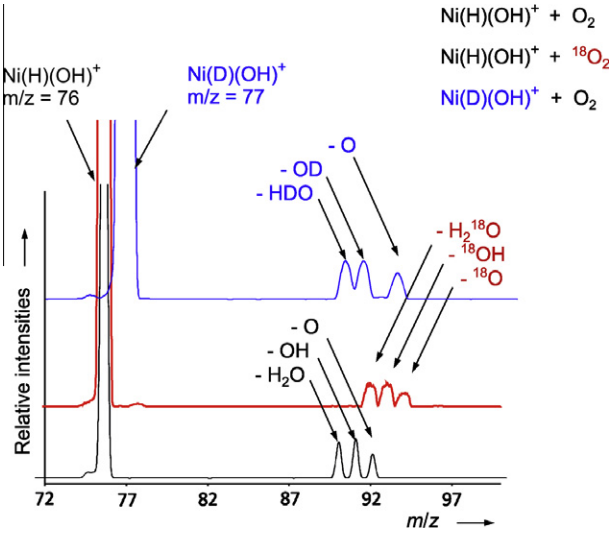

Fig. 7. Thermal ion/molecule reactions of mass-selected $Ni(H)(OH)^+$ with O_2. Black line with $^{16}O_2$, red line with $^{18}O_2$, and blue line $^{16}O_2/Ni(D)(OH)^+$ (adapted from Ref. [68]).

The remarkable, if not unique behavior of $Ni(H)(OH)^+$ toward CH_4 and O_2 has triggered quite some interest among theoreticians. Earlier DFT-based work [33] had already suggested that the quartet state of $Ni(H)(OH)^+$ is *ca.* 80 kJ mol^{-1} less stable than its doublet electromer; further, the latter undergoes a barrier-free isomerization to the global minimum, i.e., the chemically inert $Ni(H_2O)^+$ complex. This analysis has been confirmed later and extended by more elaborate calculations [70]. Thus, the quartet state of $Ni(H)(OH)^+$ is the reactive species, and it must have a lifetime long enough to undergo the thermal ion/molecule reactions with O_2 and CH_4. However, one rightly wonders what may prevent this high-energy quartet state from spontaneously undergoing intersystem

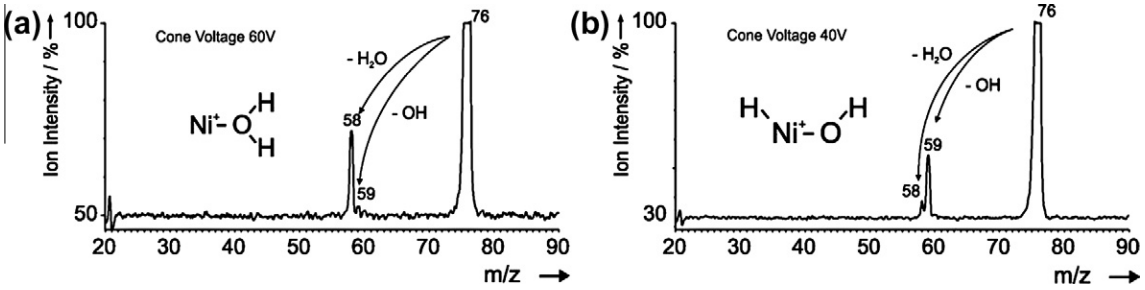

Fig. 5. CID mass spectra of (a) $Ni(H_2O)^+$ complex and (b) $Ni(H)(OH)^+$ (adapted from Ref. [66]).

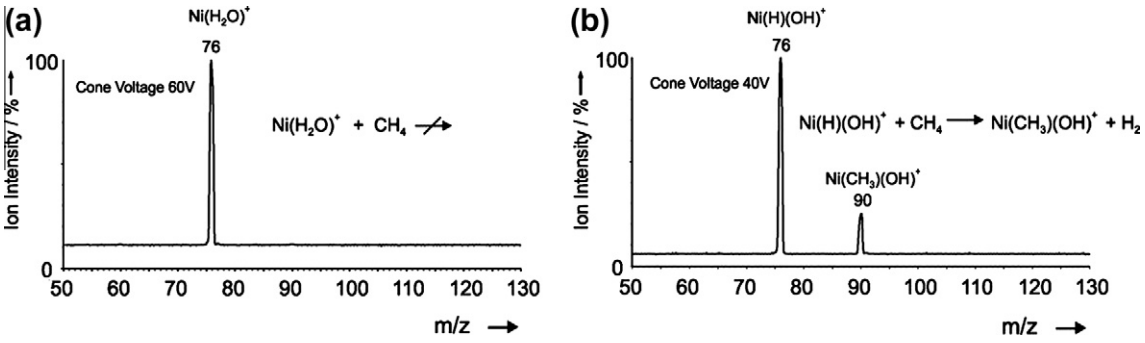

Fig. 6. ESI mass spectra of (a) $Ni(H_2O)^+/CH_4$ and (b) $Ni(H)(OH)^+/CH_4$ at room temperature (adapted from Ref. [66]).

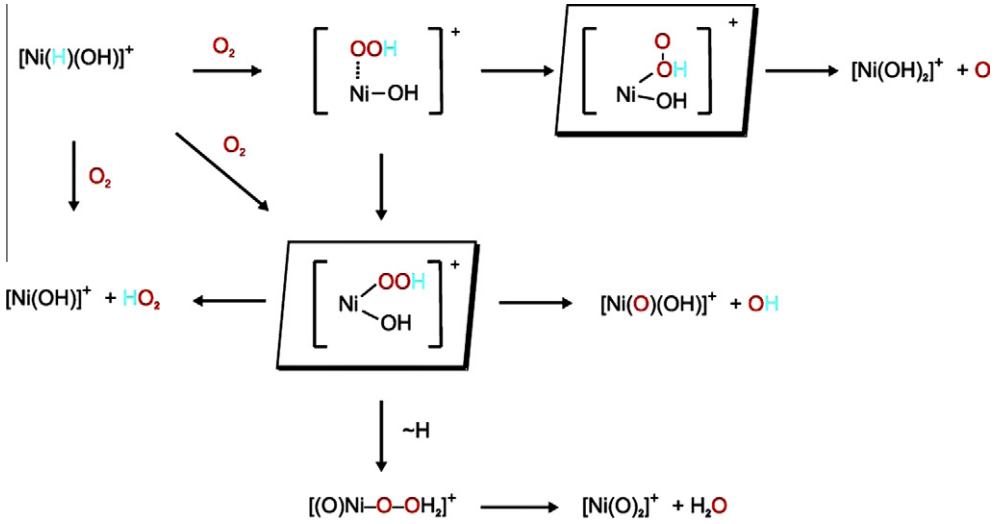

Scheme 3. Network of O_2-activation by $Ni(H)(OH)^+$ (adapted from Ref. [68]).

crossing to the much more stable doublet electromer. Theoretical work based on DFT using various functionals, coupled-cluster, and MCSCF calculations reveals an entirely unexpected electronic structure such that the hydroxyl ligand in $Ni(H)(OH)^+$ behaves as a redox non-innocent ligand [71] and becomes oxidized to formally afford an electronic structure that is consistent with a Ni^{II}–$(OH)^{\cdot}$ species rather than the more traditional Ni^{III}–$(OH)^-$assignment. As a result, the doublet and quartet states are not related by a simple, single spin flip; consequently, the intersystem crossing becomes inhibited. This is further indicated by unexpectedly small spin-orbit coupling constants. Lifetime estimates based on Landau-Zener schemes predict a minimal lifetime of the excited quartet state of $Ni(H)(OH)^+$ of a few microseconds; this lifespan is more than sufficient to permit the truly unique gas-phase chemistry of this seemingly simple nickel complex with CH_4 and O_2.

2.2.7. Ni-based $CH_4 \rightarrow CH_3OH \rightarrow CH_2O$ conversions

The intriguing mechanistic aspects of these economically extremely important conversions [72] which for a long-time were regarded as a sort of a mechanistic conundrum have been resolved recently [13]; in some systems, e.g., FeO^+/CH_4, a TSR scenario matters in the catalytic cycle in particular in the step $MO^+ \rightarrow (CH_3)$-$M(OH)^+$, Scheme 4 [73–76].

More recently, the room-temperature chemical kinetics has been measured for the catalytic activity of Group 10 atomic cations (Ni^+, Pd^+, and Pt^+) in the $CH_4 \rightarrow CH_3OH$ conversion with ozone, and Ni^+ was found to be the most efficient catalyst [77]. Also, metal-oxide (NiO, FeO, CuO) doped zeolites were suggested as promising candidates for the direct methane → methanol conversion [13,78–80]. In fact, even "naked" CuO^+ brings about this reaction at room temperature with high efficiency [81], and the couple CuO^+/CH_4 demonstrates how the spin state controls the chemoselectivity, i.e., H-atom from CH_4 vs. O-atom transfer from CuO^+ to CH_4.

In the mechanistic understanding of the $CH_3OH \rightarrow CH_2O$ oxidation, the relevant questions center around the following topics: (1) In the initial step, Scheme 5., does a metal-based mediator [M] induce preferentially a cleavage of the stronger O–H or the weaker C–H bond of CH_3OH and (2) for a given sequence of events, which of the two hydrogen-atom transfer steps constitutes the rate-determining one? As these questions have been dealt with quite comprehensively in a recent Review [13], here we will mention briefly only a few Ni-related examples which demonstrate once more the rather unique role that this element also plays in this context.

As shown in Fig. 8 and supported by additional experiments as well as extensive DFT-based calculations [82,83], ESI of methanolic solutions of MX_2 (M = Fe, Co, Ni; X = Br, I) brings about exclusive activation of the O–H group for iron, while the nickel precursor specifically cleaves the C–H group to form $Ni(CH_2OH)^+$. For the cobalt system, one encounters an intermediate situation with a slight preference for the generation of the methoxy complex $Co(OCH_3)^+$ in competition with generating $Co(CH_2OH)^+$.

Mechanistic insight into the origin of the bond-selective, metal-dependent CH_3OH activation has been gathered from DFT calculations and by establishing experimentally the precursors from which the $[M,C,H_3O]^+$ species originate upon ESI of MX_2/CH_3OH solutions [82,83]. For iron, the $Fe(OCH_3)^+$ product is due to sequential evaporation of up to eight CH_3OH molecules from $Fe(OCH_3)(CH_3OH)_n^+$ ($n \leqslant 8$), and the latter is generated via solvolysis of FeX_2 by the nucleophilic CH_3OH solvent. Moreover, high-spin $Fe(OCH_3)^+$ is, according to the DFT calculations, 69 kJ mol^{-1} more stable than the quintet isomer $Fe(CH_2OH)^+$. For the co-generation of isomeric $[Co,C,H_3,O]^+$, two pathways have been identified. The one, leading to the methoxy complex $Co(OCH_3)^+$, is analogous to that for the iron system starting from $Co(OCH_3)(CH_3OH)_n^+$ ($n \leqslant 8$). However, this precursor, in competition with sequential CH_3OH

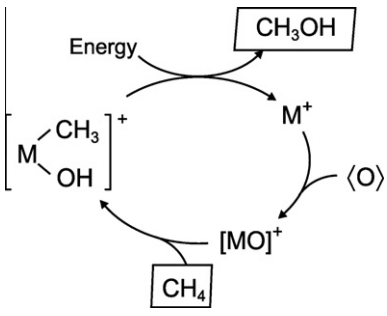

Scheme 4. Catalytic cycle for the homogeneous $CH_4 \rightarrow CH_3OH$ conversion with an oxygen equivalent ⟨O⟩, e.g. N_2O or O_3, mediated by atomic metal cations.

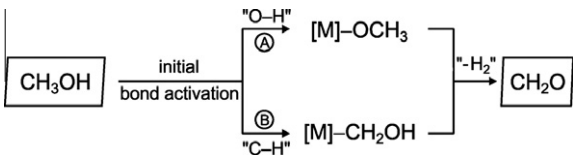

Scheme 5. Pathways for a metal-mediated $CH_3OH \rightarrow CH_2O$ conversion.

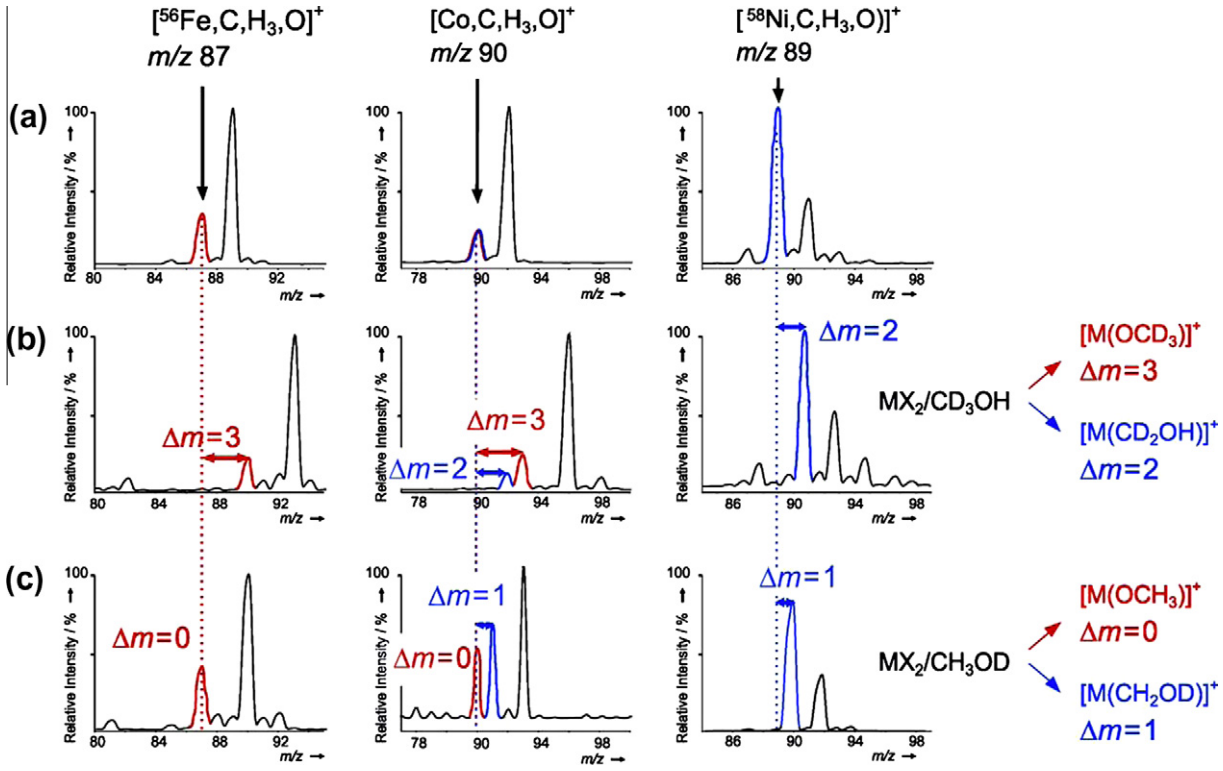

Fig. 8. Partial ESI source spectra of the Fe, Co, and Ni halides MX_2 (X = Br, I) dissolved in (a) CH_3OH/H_2O, (b) CD_3OH/H_2O, and (c) CH_3OD/D_2O. (Adapted from Ref. [82]).

evaporation, undergoes also loss of CH_2O and CH_3OH to generate $Co(H)(CH_3OH)^+$. This intermediate, in a spin-allowed elimination involving the Co–H bond and a hydrogen atom from the methyl group of CH_3OH, then decomposes to H_2 and a quartet state of $Co(CH_2OH)^+$; the latter is 25 kJ mol^{-1} higher in energy than ground-state $Co(OCH_3)^+$ having the same multiplicity. For the exclusive generation of $Ni(CH_2OH)^+$, two pathways were identified, both involving $Ni(X)(CH_3OH)^+$ (X = H, Br) as immediate precursors; in the subsequent evaporation of HX, the hydrogen atom originates from the methyl group of CH_3OH. DFT calculations, Fig. 9, are not only consistent with the experimental observations but also explain why $Ni(CH_2OH)^+$ is formed rather than the thermochemically slightly more favorable $Ni(OCH_3)^+$ isomer. Here, the crucial point is that starting from ground-state triplet $Ni(H)(CH_3OH)^+$ (^{3}**15**), the spin-allowed reaction to produce $^3Ni(OCH_3)^+$ via ^{3}TS**15/16** cannot compete energetically with a reaction which, after spin inversion ^{3}**15** → ^{1}**15**, proceeds via ^{1}TS**15/17** toward $^1Ni(CH_2OH)^+$.

Recently, it was observed that not only the nature of the metal but, for a given metal, also the ligand L matters with regard to the course of C–H vs. O–H bond activation of CH_3OH [84]. For example, in the ion/molecule reactions of NiL^+ with CD_3OH the ratio HL vs. DL loss amounts to 33 : 1 (L = OH), for the electronically related $NiCl^+/CD_3OH$ system it drops to 2:1, and for $NiBr^+/CD_3OH$ it is <0.05! Clearly, an understanding of this unusual ligand effects requires further detailed theoretical investigations. As exploratory DFT studies already reveal, the strong dependence on the functionals used suggests to employ more sophisticated wave-function-based methods.

3. Homo- and heteronuclear nickel-containing cluster ions

3.1. General considerations

Among the principal motivations why to engage in studying the gas-phase chemistry and physics of metal clusters, the most often quoted ones include: (i) Clusters may serve as tractable models for surfaces and heterogeneous catalysis and (ii) clusters generally exhibit unique reactivity and unusual properties. The first of these two factors is perhaps the most important one and is reasonable on the ground that highly dispersed metals or surface defect sites are coordinatively and electronically as unsaturated as "naked" clusters are. Further, quite a few gas-phase studies with mass-selected clusters indicate that as the cluster size increases, the chemistry rapidly reaches a behavior comparable to that of a bulk phase. These and other observations are consistent with the concept that, in a first approximation, chemical bonds are "more localized" phenomena, in contrast to global quantities such as ionization energies or electron affinities.

A pertinent concern with regard to the studies of *charged* gas-phase species is their actual relevance to real-world catalysis; fortunately, there exists a few examples demonstrating that the fundamental chemistry is relatively insensitive to the charge state of the metal, provided the cluster size is not too small. This is perhaps a consequence of the fact that the charges are highly delocalized over the metal cluster resulting in no particularly strong charges at a given atom or point of the cluster surface. Also, the thermodynamic stabilities, e.g., bond energies of neutral and cationic transition-metal clusters exceeding a particular size are often the same; moreover, for some systems there exists an excellent correspondence between ligands bound to a transition-metal cluster cation or a neutral single-crystal surface. Clearly, differences are known to exist as well, and understanding their origin(s) can be advantageous [85].

3.2. Selected examples for cluster-size effects on thermochemical features and reactivity

The experimental values for the binding of a hydrogen atom to various nickel surfaces center around 2.72 eV, and guided ion-beam experiments of mass-selected Ni_n^+ (n = 2–16) with D_2

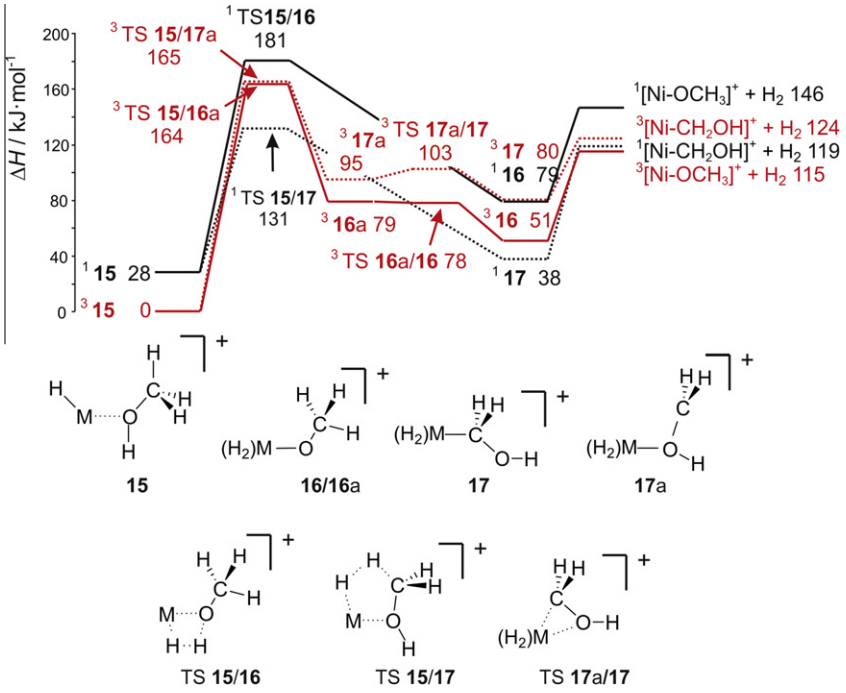

Fig. 9. Potential-energy surface for the bond activation of methanol starting from triplet (red lines) and singlet (black lines) precursors $^{1,3}Ni(H)(CH_3OH)^+$ (^{1,3}**15**). The reaction paths involving O–H bond and C–H bond activations are shown in continuous and dashed lines, respectively. Both structures **16** and ^{3}**16**a correspond to $Ni(OCH_3)(H_2)^+$ complexes with the H–H bond parallel and perpendicular to the NiOC plane, respectively; no bond activation is involved in ^{3}**TS16**a/**16**. ^{3}**TS17**a/**17** corresponds to a haptotropic metal shift from the oxygen to the carbon atom of the CH_2OH ligand. Relative energies are given in kJ mol^{-1}. (Adapted from Ref. [83]).

demonstrate that the Ni_n^+–D bond energies for larger clusters ($n \geqslant 11$) are close to that for bulk nickel phases [86]. From beam experiments of Ni_n^+ (n = 2–18) with O_2, size-dependent bond energies could be derived and a comparison with bulk-phase thermochemistry suggests that binding of oxygen in threefold sites dominates in these small nickel-cluster ions [87]. Studies of the kinetic-energy dependences of the endothermic reactions of Ni_n^+ (n = 2–16) with CD_4 provided the bond energies for nickel-cluster cations to C, CD, CD_2, and CD_3 [88]. The relative magnitudes in bond energies of these ligand fragments are consistent with simple bond-order considerations (triple, triple, double, and single bond orders, respectively). These data which are in reasonable agreement with theoretically derived numbers [89] and which, for larger cluster sizes, rapidly reach relatively constant values may provide reasonable estimates for heats of adsorption of molecular carbon-based fragments to nickel surfaces data which are difficult to obtain otherwise. For the metal-mediated dehydrogenation of ethylene ($C_2H_4 \rightarrow C_2H_2 + H_2$), there seems to exist a good correlation between the nickel-clusters' size-dependent ionization energies and the cross-section for dehydrogenation. For Ni_n^+ clusters (n = 3–30), it was found that for cluster sizes n > 10, the clusters already exhibit a bulk-like electronic structure [90]. In contrast, the adsorption and chemical degradation of methanol on Ni_n^+ clusters (n = 3–11) changes dramatically with the cluster size [91]. For example, demethanation proceeds preferentially on Ni_n^+ , carbide formation on $Ni_{7,8}^+$, and chemisorption on Ni_6^+ . A detailed kinematic modeling taking into account barrier heights between physi- and chemisorbed states of the molecule as well as geometrical details of the cluster structures helped to explain these remarkable observations. In the context of the industrially important CO oxidation, the effects of charge states, stoichiometries, and structural aspects of nickel oxide clusters have been addressed [92]. Anionic clusters with a stoichiometry containing one more oxygen than nickel atom, e.g., $Ni_2O_3^-$ and $Ni_4O_5^-$, were found to be rather reactive in the O-atom transfer to CO. In contrast, cationic nickel oxide clusters react preferentially through the adsorption of CO onto the cluster accompanied by the evaporation of O_2 or cluster degradation. Genuine catalytic cycles have been reported for the reaction of $Ni_2O_2^+$, generated from N_2O and Ni_n^+ , with CO and small hydrocarbons (e.g., ethane, propane, and *n*-butane), and the increased reactivity of $Ni_2O_2^+$ in comparison with $Mn_2O_2^+$ or $Fe_2O_2^+$ has been ascribed to a lower oxygen-binding energy in the nickel cluster [93].

3.3. Homo- and heteronuclear 3d metal-dimer cluster cations M_2^+ and $M'M^+$

The observations that (i) Ni_2^+ in contrast to most other 3d cluster dimers $M'M^+$ brings about thermal activation of C_2H_6, a process which does not take place with atomic Ni^+, and (ii) NiM^+ dimers (M = Fe, Co, Ni) exhibit in the initial step selective C–H rather than competitive C–H *and* C–C bond activation of linear alkanenitriles [94] point to a particular role *nickel*-containing clusters might play. This is indeed the case as shown in the remarkable chemistry these clusters exhibit when reacted with cyclohexane [28]. As already mentioned (Section 2.1), some of the *atomic* 3d transition-metal cations undergo highly face-selective dehydrogenation of this substrate. In analogous reactions of homonuclear M_2^+ (M = Ti, V, Cr, Mn, Fe, Co, Ni, and Cu), heteronuclear nickel-containing clusters NiM^+ (M = Ti, Mn, Fe, Co, Cu, and Al) and also $CoCu^+$ one observes exclusive C–H bond activation resulting in the elimination of up to nH_2 (n = 1–4). The data are summarized in Tables 1 and 2.

For any reaction channel observed with *c*-C_6H_{12}, none of the dimeric cations give rise to products indicative for C–C bond activation; instead, only single or multiple dehydrogenations take place. Furthermore, relatively efficient dehydrogenation is reserved for three of the eight homonuclear clusters investigated, namely for Ti_2^+, Ni_2^+, and Cu_2^+; for the remaining dimers V_2^+, Cr_2^+, Mn_2^+, Fe_2^+, and Co_2^+, dehydrogenation occurs either only sluggishly (V_2^+, Cr_2^+, and Fe_2^+) or does not take place at all (Mn_2^+ and Co_2^+). In contrast, heteronuclear dimers of nickel combined with a late transition metal – except for $NiFe^+$ – i.e., $NiCo^+$ and $NiCu^+$ show almost the same

Table 1
Branching ratios[a] of the neutral losses, relative rate constants, and efficiencies (ϕ) in the reactions of mass-selected, homonuclear M_2^+ cations (M = Ti, V, Cr, Mn, Fe, Co, Ni, Cu) with cyclohexane.

M	$-H_2$	$-2H_2$	$-3H_2$	$-4H_2$	k_{exp}[b]	ϕ[c]
Ti		8	90	2	4.2	36
V			100		0.2	2
Cr		100			0.03	0.3
Mn	–	–	–	–	<0.001	
Fe			100		0.005	0.02
Co	–	–	–	–	<0.001	
Ni		5	95		9.3	83
Cu	100				2.5	23

[a] Normalized to a sum of 100.
[b] Given in 10^{-10} cm^3 s^{-1} molecule^{-1}.
[c] Given in %.

Table 2
Branching ratios[a] of the neutral losses, relative rate constants, and efficiencies (ϕ) in the reactions of mass-selected, heteronuclear NiM^+ cations (M = Ti, Mn, Fe, Co, Cu, Al), and of $CoCu^+$ with cyclohexane.

M′M$^+$	$-H_2$	$-2H_2$	$-3H_2$	k_{exp}[b]	ϕ[c]
NiTi		75	25	5.8	51
NiMn	90	4	6	0.9	8
NiFe			100	0.01	0.1
NiCo		13	87	6.9	62
NiCu		20	80	9.3	85
NiAl		65	35	8.8	73
CoCu		26	74	7.1	65

[a] Normalized to a sum of 100.
[b] Given in 10^{-10} cm^3 s^{-1} molecule^{-1}.
[c] Given in %.

high efficiency toward C–H bond activation of cyclohexane as homonuclear Ni_2^+. Likewise, also the branching ratios of double vs. triple dehydrogenation are similar, with triple dehydrogenation being the major reaction channel. Interestingly, also $CoCu^+$, which is isoelectronic with Ni_2^+, brings about efficient dehydrogenation with the liberation of up to $3H_2$. Note the distinct behavior of their homonuclear brothers: for Co_2^+ no reaction is observed, and for Cu_2^+ only single dehydrogenation takes place with a much smaller efficiency when compared to $CoCu^+$. Apparently, 19 valence electrons in the valence shell of the 3d dimers may be favorable for reactivity. However, electron count alone is not sufficient to explain the reactivity pattern, as the 18 electron systems $FeCu^+$ and $NiCo^+$ differ significantly with respect to reactivity. According to the early work of Freiser and co-workers [95], $FeCu^+$ is unreactive with linear (C_1–C_6) and cyclic (C_3–C_6) alkanes while $NiCo^+$ efficiently dehydrogenates cyclohexane (see Table 2). What is also remarkable and cannot be elucidated yet only based on the present gas-phase experiments is the non-reactivity of $NiFe^+$ in comparison with the highly reactive $NiCo^+$ and Ni_2^+ cluster cations, or, in other words: it is not clear which electronic factors make the nickel-containing cationic dimers so special and distinct. That nickel often (but not always) plays an outstanding role in these diatomic heteronuclear clusters is also indicated by the efficient thermal dehydrogenation of C_2H_6 mediated by NiM^+ (M = Ni, Cu, Al) [28]. While these three heteronuclear cluster ions exhibit high efficiency (and for the case of $NiAl^+$ also high regioselectivity resulting in quantitative HD loss from CH_3CD_3), combinations of Ni^+ with Ti, Mn, Fe, and Co are practically non-reactive toward this substrate [28].

Back to *c*-C_6H_{12}. In the reaction with *c*-C_6H_{12}, the combination of nickel with a *3d* metal onward the left side of the periodic table, i.e., $NiMn^+$ and $NiTi^+$ leads again to a successive reactivity increase. However, in terms of chemoselectivity, the main reaction channel for $NiTi^+$ corresponds to double instead of triple dehydrogenation in contrast to Ni_2^+ and Ti_2^+; for the latter cluster, even fourfold dehydrogenation is observed. In contrast, for $NiAl^+$, which features a high efficiency, only single- and double dehydrogenation take place. Again, for a coherent explanation and understanding of these puzzling findings rather thorough theoretical studies are warranted.

To shed some light on possible reaction mechanisms, the study of ion/molecule processes of the cluster ions with [*all-cis*-1,2,3,4,5,6-D_6]-cyclohexane proved useful, Table 3.

From the data reported in Table 3, it is obvious that face selectivity, as observed for most of the *atomic* 3d cations, is not always preserved for the dimeric clusters. For example, complete scrambling of all 12 H/D atoms occurs in the reaction of $C_6H_6D_6$ with Ti_2^+ as indicated by the good agreement between the experimental and computational data for triple hydrogen (deuterium) loss. Also,

Table 3
Isotope patterns[a] of double and triple dehydrogenation in the reactions of [*all-cis*-1,2,3,4,5,6-D_6]-cyclohexane with M′M$^+$.

M′M$^+$	Ni_2	Ni_2[b,c]	NiTi[d]	NiCo[c]	NiCu[c]	NiAl[c]	CoCu[c]	Ti_2[e,f]
$-2H_2$	3	3 (8)	43 (45)	3 (4)	3 (7)	24 (27)	10 (10)	
$-[H_3,D]$			4 (6)					
$-[H_2,D_2]$	1		8					
$-[D_3,H]$			4 (3)					
$-2D_2$	8	9 (5)	12 (11)	10 (10)	19 (15)	18 (15)	27 (29)	
$-3H_2$	52	61 (60)	21 (15)	77 (77)	50 (53)	49 (49)	54 (49)	10 (7)
$-[H_5,D]$			2 (0)					27 (28)
$-[H_4,D_2]$	7		4 (2)					32 (37)
$-[H_3,D_3]$			0 (3)					20 (21)
$-[H_2,D_4]$	6		1 (1)					11 (6)
$-[H,D_5]$			0 (0)					0 (1)
$-3D_2$	23	27 (27)	1 (6)	10 (9)	28 (25)	9 (9)	9 (12)	0 (0)
k_1/k_2		0.11		0.03	0.03	0.36	0.04	
k_{rad}/k_2		1.01		1.43	1.73	0.99	1.77	
KIE		1.21	1.28	1.43	1.11	1.33	1.10	2.58

[a] Given in %.
[b] Disregarding the mixed isomers.
[c] Modeled numbers according to Scheme 7 are given in parenthesis. See Ref. [28] for details of the modeling.
[d] In the modeling (numbers are given in parenthesis), face-specific dehydrogenation from one side of the ring as well as scrambling processes have been considered; the ratios are f_{spec} = 76% and f_{scr} = 24%, respectively. The ratio for double dehydrogenation of one face of the carbon ring combined with single dehydrogenation of the opposite side has been fitted to 0%.
[e] Due to the low intensity of the corresponding signals, double- and fourfold dehydrogenation have been neglected.
[f] Numbers derived from modeling are given in parenthesis; a complete scrambling of all H/D positions of [*all-cis*-1,2,3,4,5,6-D_6]-cyclohexane with a KIE of 2.58 has been assumed.

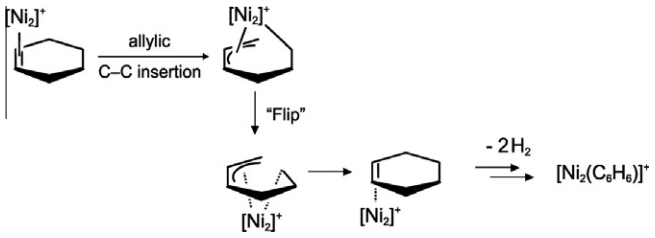

Scheme 6. Stereoselective dehydrogenation of *two* faces of the cyclohexane ring.

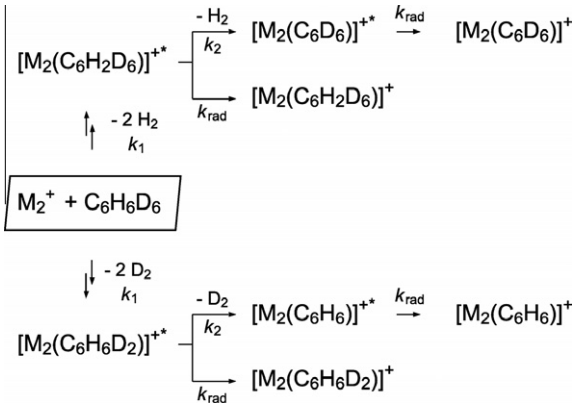

Scheme 7. Kinetic scheme for radiative cooling in competition with consecutive dehydrogenation of [D_6]-cyclohexane with dimeric metal cluster ions M_2^+.

of quite some mechanistic interest are the findings for Ni_2^+. The eliminations of some "H_2D_4" and "H_4D_2" (in addition to the major losses of "D_6" and "H_6") demonstrate that triple dehydrogenation is not restricted exclusively to the face of the substrate on which the reaction commences; however, the absence of signals indicative for "H_5D," "H_3D_3," or "HD_5" rule out a classical equilibration of the two sides. Conceivably, after the first dehydrogenation allylic C–C bond activation, followed by a ring flip and de-sertion of the Ni_2-cluster, the activating Ni_2^+-species is capable to operate on two faces of the cyclohexane ring, Scheme 6. However, in the actual formation of each pair of molecular hydrogen only atoms from the *same* face are involved, thus accounting for the elimination of even-numbered H_nD_m from [*all-cis*-1.2.3.4.5.6.-D_6]-cyclohexane.

To model the experimentally determined isotope patterns of double and triple dehydrogenation by the clusters Ni_2^+, $NiAl^+$, $NiCo^+$, $NiCu^+$, and $CoCu^+$, a rather detailed kinetic scheme had to be considered. For these five dimers, the experimental data for double dehydrogenation, given in Table 3, suggest a higher and, thus a faster rate for the loss of $2D_2$ vs. $2H_2$, which implies the operation of an *inverse* KIE. Inverse KIEs are typically found for secondary KIEs and are often caused by a change in hybridization from sp^2 to sp^3. As in the present system dehydrogenation of the substrate changes the hybridization of the carbon atoms from sp^3 to sp^2, the phenomenologically observed higher degree of $2D_2$ vs. $2H_2$ eliminations is, more likely, not based on an inverse KIE, but rather on the fact that the expulsion of H_2 from $M'M(C_6H_2D_6)^+$ (mandatory for face selectivity) proceeds faster than the loss of D_2 from $M'M(C_6H_2D_6)^+$. This, again, is not necessarily caused by an intrinsically high KIE for the third dehydrogenation but is more likely the result of an increased lifetime of the rovibrationally excited $M'M^+/D_2$-cyclohexadiene intermediate. As the third dehydrogenation is subject to a KIE, the presence of a sizeable isotope effect may cause an isotopically sensitive branching [96–101] in the competition between dehydrogenation and radiative cooling [102,103]. This way of reasoning has been taken into account in the modeling of the experimental data, Scheme 7; here k_1 being the combined rate constant for the first and second dehydrogenation, k_2 represents the rate constant of the third dehydrogenation, and k_{rad} stands for the radiative cooling of the $M'M^+$/cyclohexadiene intermediate, respectively. As shown in Table 3, the agreement with the experimental data is quite pleasing.

As the H/D scrambling processes, indicated by the elimination of *odd* numbers of H/D atoms in molecular hydrogen liberated, cannot be explained by a ring-flip mechanism, Scheme 6, a different scenario has to be invoked. The fact that both neutral and cationic *early* 3d metal clusters tend to form multiple sandwich complexes with benzene, e.g., M-C_6H_6-M [104–106], may suggest that the metal–metal bond of the Ti_2^+ cluster will be cleaved at some stage of the multiple dehydrogenation sequence with the two metal atoms then moving to different faces of the cyclohexene ring; after a sequence of β-H(D) and *retro* β-H(D) transfers, the release of HD is possible. A conceivable scenario is suggested in Scheme 8.

While various mechanistic features of the metal-mediated dehydrogenation of cyclohexane remain to be clarified, the data presented here clearly point to the extraordinary rich variability of small cluster units that awaits to be exploited. This holds true also for the rather selective, remote C–H bond activation of flexible linear alkanenitriles, brought about by homo- and heteronuclear cluster cations $M'M^+$ ($M'M$ = Fe, Co, Ni) [94]. In comparison with atomic cations, these diatomic clusters react more specifically and only insert in C–H bonds in the initial step, whereas bare atomic M^+ activates both C–H and C–C bonds. Like for M^+, dehydrogenation proceeds via remote functionalization [29,30] of the terminal positions of the substrate [94]. Once more, nickel exhibits some special features in that only the Ni-containing clusters Ni_2^+ and $NiCo^+$ bring about double dehydrogenation as well as C–C bond activation after the first dehydrogenation.

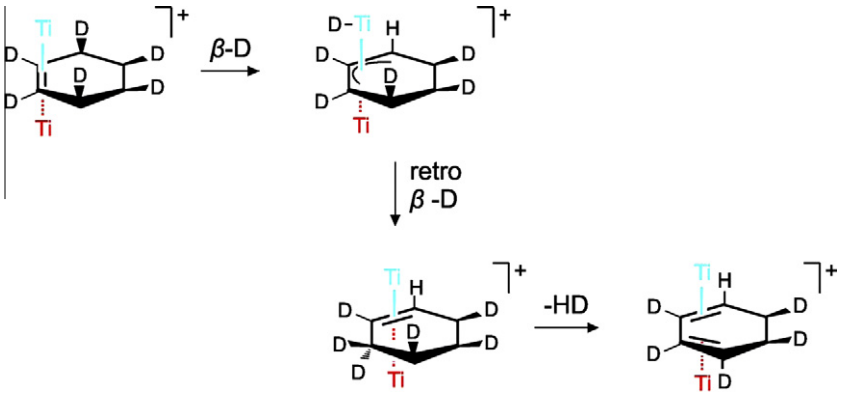

Scheme 8. Hydrogen/deuterium scrambling involving *different* faces of the cyclohexane ring.

As stated in footnote 1 and underlined by the examples discussed in this article, the element nickel deserves to be regarded as a rather distinguished member among 3d transition metals [28]; future work with an emphasis on both gas-phase ion spectroscopy and reliable electronic structure calculations is indicated to shed further light on the amazing chemistry these species exhibit.

Acknowledgments

Generous support of this research by the *Fonds der Chemischen Industrie* and the "Cluster of Excellence: Unifying Concepts in Catalysis," funded by the *Deutsche Forschungsgemeinschaft* and administered by the *Technische Universität Berlin* is gratefully acknowledged.

References

[1] G. Ertl, Reactions at Solid Surfaces, Wiley, Hoboken, 2009.
[2] K. Koszinowski, D. Schröder, H. Schwarz, J. Am. Chem. Soc. 125 (2003) 3676.
[3] K. Koszinowski, D. Schröder, H. Schwarz, Organometallics 23 (2004) 1132.
[4] K. Koszinowski, D. Schröder, H. Schwarz, Angew. Chem. Int. Ed. 43 (2004) 121.
[5] K. Eller, H. Schwarz, Chem. Rev. 91 (1991) 1121.
[6] D. Schröder, C. Heinemann, W. Koch, H. Schwarz, Pure Appl. Chem. 69 (1997) 273.
[7] V.E. Bondybey, M.K. Beyer, J. Phys. Chem. A 105 (2001) 951.
[8] D.K. Bohme, H. Schwarz, Angew. Chem. Int. Ed. 44 (2005) 2336.
[9] G.E. Johnson, E.C. Tyo, A.W. Castleman Jr, Proc. Natl. Acad. Sci 105 (2008) 18108.
[10] G.E. Johnson, R. Mitrić, V. Bonačić-Koutecký, A.W. Castleman Jr, Chem. Phys. Lett. 475 (2009) 1.
[11] M. Schlangen, H. Schwarz, Dalton Trans. (2009) 10155.
[12] J. Roithová, D. Schröder, Chem. Rev. 110 (2010) 1170.
[13] H. Schwarz, Angew. Chem. Int. Ed. 50 (2011), doi:10.1002/anie.201006424 (and numerous references therein).
[14] D. Hasenberg, L.D. Schmidt, J. Catal. 97 (1986) 156.
[15] R. Horn, G. Mestl, M. Thiede, F.C. Jentoft, P.M. Schmidt, M. Bewersdorf, R. Weber, R. Schlögl, Phys. Chem. Chem. Phys. 6 (2004) 4514.
[16] P. Sabatier, J.P. Senderens, C. R. Acad. Sci. Paris 134 (1902) 514.
[17] J.P. Hindermann, G.J. Hutchings, A. Kiennemann, Catal. Rev. Sci. Eng. 35 (1993) 1.
[18] M.E. Dry, Appl. Catal. A. Gen. 276 (2004) 1.
[19] K. Ziegler, H.G. Gellert, E. Holzkamp, G. Wilke, Brennstoff Chem. 321 (1954) 35.
[20] G. Wilke, Angew. Chem. Int. Ed. Engl. 27 (1988) 185.
[21] G. Wilke, Angew. Chem. Int. Ed. 42 (2003) 5000.
[22] P. Heimbach, Angew. Chem. Int. Ed. Engl. 12 (1973) 975.
[23] J. Montgomery, Acc. Chem. Res. 33 (2000) 467.
[24] S.-I. Ikeda, Acc. Chem. Res. 33 (2000) 511.
[25] An entire issue of Tetrahedron is devoted to modern, nickel-based catalysis; see: T.F. Jamison, Tetahedron 62 (2006) 7499.
[26] A. Sigel, H. Sigel, R.K.O. Sigel, Nickel and its Surprising Impact in Nature, vol. 2, Wiley & Sons, West Sussex, UK, 2007.
[27] The term "das 'nackte' Nickelatom" (the "naked" nickel atom) has been coined by Professor G. Wilke; see, for example: G. Wilke, Angew. Chem. 75 (1963) 10.
[28] M. Schlangen, Nickel-mediated Bond Activation of Small Alkanes and of Molecular Oxygen – Ligand Effects and the Role of the Metal's Formal Oxidation State; Ph.D. Thesis, Dissertation D83, Technische Universität Berlin, 2008.
[29] R. Breslow, Acc. Chem. Res. 13 (1980) 170.
[30] H. Schwarz, Acc. Chem. Res. 22 (1989) 282.
[31] P.B. Armentrout, J.L. Beauchamp, Chem. Phys. 50 (1980) 37.
[32] P. Cheng, G.K. Koyanagi, D.K. Bohme, J. Phys. Chem. A 111 (2007) 8561.
[33] A. Irigoras, O. Elisalde, I. Silanes, J.E. Fowler, J.M. Ugalde, J. Am. Chem. Soc. 114 (2000) 114.
[34] O. Lakuntza, J.M. Matxain, J.M. Ugalde, Chem. Phys. Chem. 11 (2010) 3172.
[35] D.E. Clemmer, P.B. Armentrout, J. Phys. Chem. 95 (1991) 3084.
[36] Q. Zhang, P.R. Kemper, M.T. Bowers, Int. J. Mass Spectrom. 210/211 (2001) 265.
[37] A. Shayestek, V.V. Lavov, G.K. Koyanagi, D.K. Bohme, J. Phys. Chem. A 113 (2009) 5602.
[38] F. Liu, X.-G. Zhang, P.B. Armentrout, Phys. Chem. Chem. Phys. 7 (2005) 1054.
[39] B.L. Kickel, P.B. Armentrout, J. Am. Chem. Soc. 117 (1995) 764.
[40] L.F. Halle, R. Houriet, M.M. Kappes, R.H. Staley, J.L. Beauchamp, J. Am. Chem. Soc. 104 (1982) 6293.
[41] M.C. Holthausen, A. Fiedler, H. Schwarz, W. Koch, J. Phys. Chem. 100 (1996) 6236.
[42] M. Blomberg, S.S. Yi, R.J. Noll, J.C. Weisshaar, J. Phys. Chem. A 103 (1999) 7254.
[43] R. Houriet, L.F. Halle, J.L. Beauchamp, Organometallics 2 (1983) 1818.
[44] M.A. Tolbert, J.L. Beauchamp, J. Phys. Chem. 90 (1986) 5015.
[45] X. Chen, W. Guo, L. Zhao, Q. Fu, Y. Ma, J. Phys. Chem. A 111 (2007) 3566.
[46] S.J. Dee, V.A. Castleberry, O.J. Villaroel, I.E. Laboren, D.J. Bellert, J. Phys. Chem. A 114 (2010) 1783.
[47] X. Chen, W. Guo, L. Zhao, Q. Fu, Chem. Phys. Lett. 432 (2006) 27.
[48] V.A. Castleberry, S.J. Dee, O.J. Villaroel, I.E. Laboren, S.E. Frey, D.J. Bellert, J. Phys. Chem. A 113 (2009) 10417.
[49] O. Blum, P. O'Bannon, D. Schröder, H. Schwarz, Organometallics 12 (1993) 980.
[50] K. Seemeyer, D. Schröder, M. Kempf, O. Lettau, J. Müller, H. Schwarz, Organometallics 14 (1995) 4465.
[51] C. Rue, P.B. Armentrout, I. Kretzschmar, D. Schröder, H. Schwarz, J. Phys. Chem. A 106 (2002) 9788.
[52] Q. Zhang, M.T. Bowers, J. Phys. Chem. A 108 (2004) 9755.
[53] M. Schlangen, H. Schwarz, Angew. Chem. Int. Ed. 46 (2007) 5614.
[54] M. Schlangen, H. Schwarz, Helv. Chim. Acta 91 (2008) 2203.
[55] P.B. Armentrout, Science 25 (1991) 1175.
[56] D. Schröder, S. Shaik, H. Schwarz, Acc. Chem. Res. 33 (2000) 139.
[57] H. Schwarz, Int. J. Mass Spectrom. 237 (2004) 75.
[58] I. Rivalta, N. Russo, E. Sicilia, J. Comput. Chem. 27 (2006) 174.
[59] J.N. Harvey, Phys. Chem. Chem. Phys. 9 (2007) 331.
[60] R.N. Perutz, S. Sabo-Etienne, Angew. Chem. Int. Ed. 46 (2007) 2578.
[61] M. Armélin, M. Schlangen, H. Schwarz, Chem. Eur. J. 14 (2008) 5229.
[62] M. Schlangen, D. Schröder, H. Schwarz, Chem. Eur. J. 13 (2007) 6810.
[63] B. Butschke, D. Schröder, H. Schwarz, Organometallics 28 (2009) 4340.
[64] B. Butschke, D. Schröder, H. Schwarz, Organometallics 29 (2010) 6002.
[65] B. Butschke, H. Schwarz, Organometallics 30 (2011) 1588.
[66] M. Schlangen, D. Schröder, H. Schwarz, Angew. Chem. Int. Ed. 46 (2007) 1641.
[67] M. Schlangen, H. Schwarz, Helv. Chim. Acta 91 (2008) 379.
[68] X. Zhang, M. Schlangen, M.-H. Baik, Y. Dede, H. Schwarz, Helv. Chim. Acta 92 (2009) 151.
[69] M.M. Gligorich, M.S. Sigman, Angew. Chem. Int. Ed. 45 (2006) 6612.
[70] Y. Dede, X. Zhang, M. Schlangen, H. Schwarz, M.-H. Baik, J. Am. Chem. Soc. 131 (2009) 12634.
[71] K. Ray, T. Petrenko, K. Wieghardt, F. Neese, Dalton Trans. (2007) 1552.
[72] G.A. Olah, A. Goeppert, G.K.S. Prakash, Beyond Oil and Gas: The Methanol Economy, Wiley-VCH, Weinheim, 2009.
[73] D. Schröder, H. Schwarz, Angew. Chem. Int. Ed. Engl. 29 (1990) 1433.
[74] D. Schröder, A. Fiedler, J. Hrušák, H. Schwarz, J. Am. Chem. Soc. 114 (1992) 1215.
[75] K. Yoshizawa, Y. Shiola, Organometallics 17 (1998) 2825.
[76] G. Altinay, M. Citin, R.B. Metz, J. Phys. Chem. A 114 (2010) 5104.
[77] A. Božović, S. Feil, G.K. Koyanagi, A.A. Viggiano, X. Zhang, M. Schlangen, H. Schwarz, D.K. Bohme, Chem. Eur. J. 16 (2010) 11605.
[78] K.A. Dubkov, V.I. Sobolev, G.I. Panov, Kinet. Catal. 39 (1998) 72.
[79] K. Yoshizawa, Acc. Chem. Res. 39 (2006) 375.
[80] E.I. Solomon, J.W. Ginsbach, D.E. Heppner, M.-T. Kieber-Emmons, C.H. Kjaergaard, P.J. Smeets, L. Tian, J.S. Woerting, Faraday Discuss. 148 (2011) 11.
[81] N. Dietl, C.v.d. Linde, M. Schlangen, M.K. Beyer, H. Schwarz, Angew. Chem. Int. Ed. 50 (2011). doi:10.1002/anie.201100606.
[82] M. Schlangen, H. Schwarz, Chem. Commun. 46 (2010) 1878.
[83] M. Schlangen, H. Schwarz, ChemCatChem 2 (2010) 799.
[84] M. Schlangen, unpublished results.
[85] P.B. Armentrout, Annu. Rev. Phys. Chem. 52 (2001) 423.
[86] F. Liu, R. Liyanage, P.B. Armentrout, J. Chem. Phys. 117 (2002) 132.
[87] D. Vardhan, R. Liyanage, P.B. Armentrout, J. Chem. Phys. 119 (2003) 4166.
[88] F. Liu, X.-G. Zhang, R. Liyanage, P.B. Armentrout, J. Chem. Phys. 121 (2004) 10976.
[89] P.E.M. Siegbahn, U. Wahlgren, in: E. Shustorovich (Ed.), Metal Surface Reaction Energetics, VCH, New York, 1991, p. 1.
[90] M. Ichihashi, T. Hanmura, T. Kondow, J. Chem. Phys. 125 (2006) 133404-1.
[91] M. Ichihashi, T. Hanmura, R.T. Cadav, T. Kondow, J. Phys. Chem. A 104 (2000) 11885.
[92] G.E. Johnson, N.M. Reilley, A.W. Castleman, Jr. Int. J. Mass Spectrom. 280 (2009) 93.
[93] K. Koszinowksi, M. Schlangen, D. Schröder, H. Schwarz, Eur. J. Inorg. Chem. (2005) 2464.
[94] M. Schlangen, D. Schröder, H. Schwarz, Helv. Chim. Acta 88 (2005) 1405.
[95] E.C. Tews, B.S. Freiser, J. Am. Chem. Soc. 109 (1987) 4433.
[96] A. Thibblin, J. Phys. Org. Chem. 1 (1988) 161.
[97] A. Thibblin, P. Ahlberg, Chem. Soc. Rev. 18 (1989) 209.
[98] U. Dreyer, D. Sülzle, D. Schröder, H. Schwarz, Helv. Chim. Acta 73 (1990) 2179.
[99] T. Prüsse, A. Fiedler, H. Schwarz, Helv. Chim. Acta 74 (1991) 1127.
[100] K. Seemeyer, T. Prüsse, H. Schwarz, Helv. Chim. Acta 76 (1993) 1632.
[101] J. Schwarz, H. Schwarz, Helv. Chim. Acta 78 (1995) 1013.
[102] R.C. Dunbar, Mass Spectrom. Rev. 11 (1992) 309.
[103] R.C. Dunbar, S.J. Klippenstein, J. Hrušák, D. Stöckigt, H. Schwarz, J. Am. Chem. Soc. 118 (1996) 5277.
[104] K. Hoshino, T. Kurikawa, H. Takeda, A. Nakajima, K. Kaya, J. Phys. Chem. 99 (1995) 3053.
[105] T. Kurikawa, H. Takeda, A. Nakajima, K. Kaya, Z. Phys. D 40 (1997) 65.
[106] P. Weis, P.R. Kemper, M.T. Bowers, J. Phys. Chem. A 101 (1997) 8207.